Available on CMS information server

CMS NOTE 2000/002

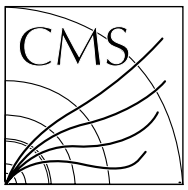

The Compact Muon Solenoid Experiment

CMS Note

Mailing address: CMS CERN, CH-1211 GENEVA 23, Switzerland

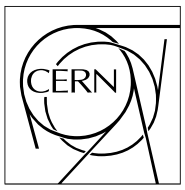

January 27, 2000

Further understanding of $PbWO_4$ Scintillator characteristics and their optimisation

LUMEN activity in 1998

S. Baccaro[1], P. Bohacek[2], B. Borgia[3], A. Cecilia[3], I. Dafinei[3], M. Diemoz[3], P. Fabeni[4], A. Festinesi[1], E. Longo[3], M. Martini[5], F. Meinardi[5], E. Mihokova[2], M. Montecchi[1], M. Nikl[2], G. Organtini[3], G.P. Pazzi[4], J. Rosa[2], M. Sulc[6], A.Vedda[5]

.

INFN - Sezione di Roma

[1]*ENEA, INN/TEC, Casaccia, Roma (Italy)*
[2]*Institute of Physics, Academy of Science, Prague (Czech Republic)*
[3]*Dip. di Fisica, Univ. La Sapienza, Roma (Italy)*
[4]*IROE-CNR, Firenze (Italy)*
[5]*INFM, Dip. Scienza dei Materiali, Univ. di Milano (Italy)*
[6]*Physics Dep., Univ. of Liberec, (Czech Republic)*

Abstract

The aim of LUMEN collaboration was the investigation on single crystals of $PbWO_4$ (PWO): the results performed up to now provide the evidence of the possibility to optimise the optical properties of an intrinsic scintillator such as PWO. The control of essential requirements in the crystal preparation (raw material purity, growing methods and post-growth annealing) as well as the introduction of selected dopants at suitable concentrations (particularly trivalent and pentavalent ions) were found to be very successful in lowering the concentration of point defects in the lattice which strongly affect scintillation properties and radiation hardness. The systematic investigation effort to better understand the scintillation characteristics and to improve the quality of PWO crystals is due to their use for the CMS electromagnetic calorimeter.

FOREWORD

This report summarizes the most important results obtained during the second part of LUMEN project activity on Lead Tungstate crystals. As outlined in the previous report (Activity of LUMEN - 1996/97) our aim was to investigate the optimization of the optical properties of PWO crystal. During this last year (1998) our task has been to complete the measurements on doping effects and give the proper feedback to the Chinese laboratories (SIC - Shanghai and BGRI - Beijing), producers of PWO crystals grown by the Bridgman technique.

Our team was directly involved in the organization of the International Workshop on Tungstate Crystals (Rome, October 12-14, 1998). This workshop was jointly organized by INFN - Sect. of Rome and ENEA – New Technology Department, Casaccia Labs. and supported by the Italian Minister of Foreign Affairs and ETH-Zurich. The objective of the workshop was to provide an overview of the state of the art in the physics and chemistry of PWO scintillating crystals and evaluate any possible improvement in the synthesis before the start of their industrial scale production for the ECAL project.

We are thankful to Prof. H. Hofer, Dr. F. Nessi-Tedaldi and Dr. P. Lecomte from Swiss Federal Institute Institute of Technology (ETH) for their cooperation which allowed us to reach significant results on Chinese crystals.

We are grateful to INFN for financial support and we thank the authors for their contributes.

Stefania Baccaro

(LUMEN Coordinator)

1. INTRODUCTION

This report summarises the most important results obtained in 1998 by the LUMEN collaboration about the study of $PbWO_4$ (PWO) scintillator characteristics and their possible improvement.

The single crystals of PWO became subject of increased interest in the nineties, because of their potential usage in detectors for High Energy Physics (HEP) experiments, namely as a scintillatng material in electromagnetic calorimeter detectors. An ideal calorimeter for HEP requires a dense, fast and radiation resistant scintillator.

The review of PWO characteristics and the results achieved by LUMEN collaboration in 1996-97 are given in Ref. 1. Simultaneous application of different experimental techniques at selected and intentionally grown PWO samples with different dopants, grown by Czochralski method from high purity raw powders and supported by sophisticated chemical analyses of as grown crystals (as GDMS and ICP) appeared very useful for the understanding of the microscopic mechanisms which determine the scintillation characteristics of PWO. At the same time, the understanding of these processes enabled to propose the way to further optimise the scintillation characteristics through the mentioned trivalent ion doping into the Pb sub-lattice.

Among the most significant results achieved by the LUMEN collaboration in this period are:

- understanding of the influence of the energy transfer processes [2, 3] and of trivalent La doping in the luminescence and scintillation decay kinetics [4];
- correlation between observed changes in the emission decay, low temperature TSL and LY characteristics [4];
- interpretation of the microscopic radiation damage mechanism consisting in the creation of two kinds of hole centres and two kinds of electron ones [5];
- explanation of the improvement of the transmission and radiation resistance of La^{3+}-doped PWO based on the coulombic compensation in the Pb-sub-lattice and resulting decrease of stable and temporary hole centres in the PWO lattice [6, 7, 8].

The aim of the LUMEN collaboration for 1998 period was concentrate further on the systematic study of the influence of trivalent dopants, and namely Lu,Y, Gd and Sc ions were studied. The comparison with Nb doping was also considered; moreover the influence of Nb and La doping on the TSL properties has been investigated by X-irradiation at 80 and 300 K, also for Russian crystals [9].

A detailed low temperature study of colour centres was performed by TSL and EPR techniques to better understand the nature of energy storage processes in PWO. On-line radiation damage measurements were performed under microtrone irradiation to study shortly living components in the induced absorption. Also, a study of the dependence of the radiation resistance of the material upon stoichiometry conditions was performed, in order to reveal congruent melt composition.

In 1998, a significant effort was also devoted to investigate the PWO crystals grown in China by Bridgman method. The most important results are reported later (see 2.2).

The investigation performed up to now on the crystals grown by Czochralski and Bridgman methods provides the evidence of the possibility to optimise the optical properties in both cases. The standard method to grow PWO single crystal is the Czochralski method. This method is currently used mainly in Bogoroditsk Techno-Chemical Plant (BTCP) (Russia), in Crytur (Czech Republic) and in Furukawa (Japan).

In Shanghai Institute of Ceramics (SIC) and in Beijing Glass Research Institute (BGRI) in China, the modified Bridgman method is used. This technique produces several ingots at the same time.

It is very important to note that both methods have merits and drawbacks, but crystals of the required quality have been grown using both technologies [10].

The processes of radiation damage and following recovery require special attention, because resulting loss of transmission, instability of light yield (LY) or even induced changes in the scintillation mechanism can strictly limit the applicability of a scintillator material in a radiation severe environment of planned detectors in LHC experiment [11].

In order to develop high quality full-size crystals, a combined effort between CMS collaboration and producers is underway to optimise mass-production of PWO crystals. Milestones for the pre-production are the understanding of the PWO scintillation mechanism necessary to enhance the light output and the comprehension of the radiation damage mechanism necessary to develop techniques to produce radiation hard crystals. The optimisation of production methods has been successfully tested on small production batches and is now ready for full-size crystals (23 cm long) [12, 13].

Extended examination of PWO characteristics (transmission, luminescence, excitation spectra as well as light yield and decay time) were performed for selected sets of PWO samples grown by Czochralski method in various plants as well as samples grown by Bridgman method in Shanghai Ceramic Institute (SIC) and Beijing Glass Research Institute (BGRI) in China. Over the past four years, the systematic R&D on the crystal growth parameters has led to a significant improvement in radiation hardness, taking into account purity of raw material and doping [5, 6, 8, 14, 15].

CMS collaboration has required the radiation hardness specifications for the three most important parameters: radiation induced absorption coefficient (μ for full saturation of crystal $\leq$ 1.5 m^{-1} at 420 nm (lateral ^{60}Co irradiation, >50 krad, >10 krad/h), Light Yield loss <6% (front ^{60}Co irradiation, 200 rad, 15 rad/h) and no recovery time constant shorter than 1 hour.

A few tens of crystals were examined and here we report only the results related to the more significant cases. The control of essential requirements in the crystal preparation (raw material purity, growing methods and post-growth annealing) as well as the introduction of selected dopants at suitable concentrations (particularly La^{3+} and Nb^{5+}) were found to be very successful in lowering the concentration of point defects in the lattice which strongly affect scintillation properties and radiation hardness [5, 6, 8, 14, 15, 16].

The doping improves the transmittance as well as the radiation hardness. A significant decrease of μ round 350 nm and 420 nm is observed for crystals doped by niobium, lanthanum, yttrium, lutetium, gadolinium [5, 6, 8, 11, 14, 15, 16] and by antimony recently [17]. Interesting results were also found using co-doping of trivalent and pentavalent ions: a significant improvement of radiation resistance was found in crystals co-doped by niobium and yttrium produced by BCTP in Russia [18] and in crystals co-doped by lanthanum and antimony produced by SIC in China. These last results will be described further on. Indeed, in this paper we will report only the most recent and important results obtained for few crystals grown by Czochralski method (see 2.1) and crystals grown by Bridgman method (see 2.2)

2. EXPERIMENTAL RESULTS AND DISCUSSION

2.1 Crystals grown by Czochralski method

2.1.1 Systematic study of the influence of trivalent dopants

2.1.1.a Lu, Y, Gd and Sc ions

A set of crystals doped with various trivalent ions as Lu, Y, Gd, Sc (at 135 ppm level in the melt before third crystallisation, at Furukawa, Iwaki, Japan) was studied by the available experimental techniques, together with an additional sample grown by adding 135 ppm of PbO in the melt (Pb-rich). The same approach already followed in the case of La doping was used, namely correlated measurements of radiation damage, LY, photoluminescence and scintillation decay, and TSL characteristics were performed.

The initial transmission, radiation induced absorption spectra and the dependence of the 420 nm induced absorption upon dose are given in Fig. 1, 2 and 3, respectively.

Selected photoluminescence (PL) decays are given in Fig. 4. Based on the PL and scintillation decay, the mean decay time was calculated and the values are given in Table I (for the details see ref. [4]). The LY values are given in the same table, as well as the true concentration of dopant ions in the samples measured by ICP technique or estimated using the knowledge of the segregation coefficients. It is worth to note that high dopant concentrations lead to a lower LY - this effect was observed mostly for Nb doping (Table I) and, to a lesser extent, in the case of Gd doping.

Selected TSL glow curves after irradiation at 90 and 295 K are given in Fig. 5 and 6, respectively. Disappearance of TSL peaks above 160 K can be noted for Lu, Y and Gd dopants; on the contrary, this effect is not observed in the case of the Sc-doped sample in which TSL structures above 160 K are detected with an

intensity even higher that in the undoped (Pb-rich) sample. Due to its small radius, this ion might be located in lattice sites different from those of Pb; alternatively, it could feature a +2 valence state similarly to what suggested in the case of the Yb ion, which also did not cause any improvement in the scintillation properties of PWO [19].

The integrals of TSL signals between 100-160 K and 100-350 K given in Table I show quantitatively the above mentioned behaviour of the glow curves. The values of the mean decay time ($\tau_{mean}=(\Sigma A_i \tau_i^2)/(\Sigma A_i \tau_i)$, A_i and τ_i stand for the pre-exponential factor and decay time of the i-th decay component, respectively) related to the photoluminescence measurements at 500 nm, to the scintillation decay (spectrally unresolved) are reported together with the values of the light yield LY and of the ratio of the integrated TSL curves from Fig. 3 over 100-160 K (I^{160}) and 100-350 K (I^{350}). True concentration of the doped ions in the crystal is reported under c_X.

Concluding, it is possible to say that Lu, Y and Gd-doped samples show very similar effects on the luminescence and scintillation characteristics with respect to the La doping investigated earlier. Namely, several times increased radiation hardness of these crystals, improved transmission around 330-500 nm, faster photoluminescence and scintillation decays and the same LY are achieved for the doping concentration around 100 molar ppm with respect to undoped (Pb-rich) crystal. On the other hand, these ions have quite different segregation coefficients in PWO (s_{Lu}=0.3, s_Y=0.8, s_{Gd}= 1.4 and s_{La}= 2.4): this allows a wide range of growth conditions, to be tested for the optimisation of the long crystal production on an industrial scale.

Finally, the Pb-rich crystal shows essentially the same characteristics with respect to previous undoped Furukawa samples reported in [4,5,7,8], which means that de-tuning of Pb/W stoichiometry of the order about 0.01 at% has no influence on the PWO crystal matrix.

2.1.1b Comparison between trivalent and Nb ions doping

The characteristics of Nb-doped samples are also given in Figs. 1-6. One should note the very high concentration of Nb ions (above 600 ppm) with respect to other dopants (Table I.). Previous attempts made at Furukava (Japan) to dope with Nb at lower levels have shown essentially no influence on the PWO characteristics [20].

The transmission spectra of unirradiated crystals are similar for La (Y,Lu,Gd) and Nb-dopings, but a lower efficiency can be noted in reducing the radiation induced absorption amplitude (Fig. 2) in the Nb-doped case; a different spectrum shape is noticed as well, which is the consequence of different charge balance processes at microscopical level for both kind of dopings [21]. An interesting difference can be further noted in the photoluminescence decays. While progressively faster decays with essentially no signal above a few hundreds nanoseconds are obtained with increasing concentration of trivalent ions, very fast initial part of the decay with a slow tail down to microsecond time scale is obtained for Nb samples (Fig.4). This confirms previous results obtained in these measurements for Bogoroditsk samples [22]. Such decay shape can be understood by considering the simultaneous existence of both a quenching of recombination decay due to high dopant concentration and an energy transfer to the WO_3 centres (Nb doping could enhance O vacancy concentration, while an opposite trend is expected for trivalent ion doping); this latter energy transfer could be responsible for enhanced slow decay tails in the green spectral part [3, 22]. Another interesting difference is noticed in TSL glow curves below RT (Fig. 5), specifically in the 200 K region. In fact, TSL peaks in this temperature range are not suppressed in the Nb-doped sample: due to the mentioned different influence of Nb and trivalent dopants, such a difference in TSL supports the hypothesis that O vacancies, acting as electron traps, are responsible for glow peaks in the 200 K region.

Concluding, while similar effects are observed as for transmission and radiation resistance improvement for the trivalent and high level Nb doping, a different behaviour is observed in emission kinetics and low-temperature TSL characteristics. These differences are most probably connected to the opposite influence of the trivalent and Nb dopings on point defects related to the O-sublattice. On the other hand, similar effects as for radiation resistance improvement for both dopings give a strong argument for the key role of Pb sublattice in the radiation damage mechanism, i.e for the key role of the stable and temporary hole states situated close to Pb sites.

2.1.1c Dependence upon Gd-concentration level

To prevent any LY loss due to high dopant concentration mentioned, the search for minimum dopant concentration was accomplished, which still efficiently reduces radiation damage, TSL peaks above 160 K and which improves the transmission course above 330 nm as well. The group of Gd-doped PWO grown in Prague was used with doping level 20, 40 and 80 molar ppm in the melt, another two samples with 60 and 135 ppm in the melt were obtained from Furukawa.

The induced absorption spectra for Prague samples is given in Fig. 7. An example of TSL characteristics above RT is given as well in Fig. 8 and the excimer laser excited decay is given in Fig. 9. An abrupt improvement of radiation resistance and diminishing of TSL peaks above RT can be noticed between 40 and 80 ppm doping level. Also the decay curve for 80 ppm sample in Fig. 9 gets noticeably faster with respect to lower doping concentration. Japanese 60 ppm sample shows only partial improvement of both TSL and radiation resistance characteristics being still 2-3 times worse with respect to 135 ppm doping level. Hence, with some safety margin, one can state the concentration round 80-100 molar ppm in the crystal as an optimum one to achieve high LY and radiation hardness and fast scintillation response simultaneously for Gd doping. Due to rather uniform influence of the trivalent dopants (La. Lu, Y and Gd) this conclusion can be generalized for all the group of the trivalent dopants mentioned.

2. 1. 2 Energy storage processes in $PbWO_4$

Thermalized electrons and holes can be localised at various traps during their diffusion towards the sites where the radiative recombination can take place (emission centres). At RT, shallow traps (with time decay in the micro-ms time scale) can just slow down their motion, giving rise to the appearance of slow components in the luminescence and scintillation decay. On the contrary, deeper traps can localise the carriers for rather long times (minutes, hours or even days) and can contribute to induced absorption phenomena, if the created centres are able to absorb the light in the spectral region of interest (near the UV/visible range in the $PbWO_4$ case). Moreover, due to their ability to storage carriers for long times, these traps can be the cause of a reduction of the light yield. The existence of these trapping sites is usually monitored by TSL or TSC techniques, which can reveal “turning points” in temperature related to the detrapping of carriers from these levels. In those cases in which an occupied trap shows an “unpaired spin”, it may be possible to characterise it in detail for symmetry, bonding features, etc. by magnetic resonance techniques (EPR, ENDOR, ODMR, etc.) and to determine more precisely its nature.

2. 1. 2.a Paramagnetic colour centres in $PbWO_4$

Previous studies dealing with TSL and EPR measurements on PWO:Mo crystals put in evidence the role of Mo impurity as electron trap below RT [23, 24], which is directly related to the appearance of slow processes in the luminescence and scintillation decay [25]. More recently, an EPR study on undoped and La-doped PWO [26] showed a new interesting feature, namely the autolocalisation of an electron at a regular W^{6+} site below 50 K, creating thus a $(WO_4)^{3-}$ centre. In Fig. 11 the most important results of ref. 26 are summarised: above 50 K $(WO_4)^{3-}$ paramagnetic centre is thermally erased and capture of released electrons at Mo impurity and at other unknown defects (U1 and U2 centres, the latter being probably a Cr impurity ion [27], in the undoped sample) occurs. In the La-doped sample, complete disappearance of U1 centre and strong increase of Mo-related EPR signal is noticed suggesting competition in electron capture between these two centres (both undoped and La-doped samples should contain comparable amount of Mo impurity well below 0.5 molar ppm according to ICP analysis). The temperature dependence of Mo-related and U1 centres does not correlate with dominant TSL peaks in the region of 100-120 K [4, 28], which indicates that these centres probably do not take part in related TSL processes, but they can be related to the TSL peaks in the 200 K region.

EPR technique completely failed in finding any paramagnetic hole centres in PWO, at variance with isostructural $CaWO_4$ in which an auto-localised hole shared between two tungsten groups ($(WO_4)_2^{3-}$) and stable up to 150 K is well known to exist [29]. One or even two-hole centres localised e.g. close to a cation (Pb) vacancy could be expected as well, as for example in MgO in which such two hole centres close to a cation vacancy were observed [30] just by EPR measurements.

2.1.2 b Correlation between EPR and TSL measurements

TSL glow curves after X-ray irradiation at 9 K, resolved in temperature and wavelength, are given in Fig. 11 for the same undoped and La-doped samples reported in 2.1.2a. Dominant TSL peak situated in the blue

spectral region occurs at a similar temperature as the above indicated disintegration of $(WO_4)^{3-}$ centre. Another peak is observed at around 95 K in the La-doped sample, which was detected also in the undoped crystal at higher doses. The analysis of the principal glow curve peak round 45 K in the undoped sample after partial cleaning revealed a very similar activation energy of about 50 meV [31] as the one determined from EPR measurements [26]. Hence correlated EPR and TSL measurements allow to conclude that around 45 K the electron is de-trapped from $(WO_4)^{3-}$ colour centre and after (short distance) diffusion it recombines with a localised hole. The absence of any TSC signal at around 45 K suggests even possible occurrence of localised recombinations between electrons and holes at luminescent sites, not involving the conduction band. The spectral position of TSL peaks in Fig. 11 reveals that the localisation of holes is either in a regular lattice site (auto-localised state) or close to a defect introducing a weak perturbation to $(WO_4)^{2-}$ groups nearby, which does not prevent their radiative de-excitation (after an electron capture) in the blue part of the spectrum (e.g. Pb vacancy could be considered in this aspect). Some differences are noticed in these two samples in the high temperature side of the 45 K peak, as a shoulder is more evident in the undoped one.

2.1.2c $CaWO_4$ and $PbWO_4$ crystals

In order to further investigate the role of the divalent cation in the scheelite PWO structure, the TSL characteristics were compared above RT for $CaWO_4$ (CWO) and PWO [32] including the influence of La doping and spectrally resolved measurements. The TSL glow curves and their spectral composition are given in Figs. 12 and 13 for PWO and CWO, respectively. Both materials show a principal glow peak at a very similar temperature around 50 ^{0}C. It can be seen that, similarly to what observed in PWO, also in CWO, the doping with trivalent La results in a lowering of this peak. Considerable difference is noticed in the spectral composition of the TSL emission (insets of Fig.'s 12 and 13). While PWO shows well defined peak in the red spectral region (see also [5, 33]), CWO emission is always situated in the blue spectral region as at low temperatures - Fig. 14.

The similarity in the glow peak position in Fig. 12 suggests the same thermal depth of the (probably electron) trap. On the contrary, due to the different spectral composition of the TSL emission in both materials (Fig.13), the recombination site itself (probably a trapped hole) should have a different origin. It is useful to note that recent band calculations [34] have shown considerable difference in the composition of the valence band (VB) top in CWO and PWO, which serve as a parent state of perturbed intrinsic hole states in general. Lowering of the TSL signal following La doping in PWO was explained by the decrease of both stable and temporary hole states related to the Pb-sublattice [4 - 8], and of O vacancies as well [21, 35]. In CWO, only influence on O vacancies and on the perturbed ($(WO_4)_2^{3-}$) hole state concentrations due to La doping can be proposed because of the absence of Ca states at the VB top. In fact, a similar concentration of La shows a quantitatively smaller effect on the 50 ^{0}C TSL peak in CWO with respect to PWO.

Concluding, the trapping levels appear to be due to point defects related to the oxygen sites both in PWO and in CWO, while Pb cations in PWO seem to be related to the creation of the recombination site (while Ca ions not) operating in the TSL above RT.

2. 1. 3 Short-living components in the induced absorption

The measurements of radiation (typically ^{60}Co) induced absorption is usually restricted in short time scale due to necessary sample transfer after irradiation. Thus only the components with recovery time above at least ten minutes can be monitored [5]. In the case of PWO crystals, 2-3 components were noted in recovery processes with recovery times from few hours to several days [36]. Recently, "on-line" measurements of transmission during irradiation at microtron facility were reported [37], which enable to monitor even build-up stage and faster (several tens of seconds) components in the recovery of transmission after switching-off the irradiation. The same idea was adopted by us for systematic scan of shortly living components in the induced absorption spectra of undoped and trivalent ion doped PWO from CRYTUR and Furukawa producers. The experimental set-up is described in [38]. The diode array transmission spectrometer equipped with high quality quartz optical fibre enabled "a snap" measurements of all the transmission spectrum in 360 - 750 nm with typical repetition each 30 s. The irradiation rates were chosen at about 5, 15 and 40 rad/min. Typical induced absorption spectrum resolved in time and wavelength is given in Fig. 15 for undoped and La-doped 15 cm long crystals. An example of cuts in time is given in Fig. 16. The presence of shortly living components showing recovery times of about a few minutes is clearly visible. The results of the analysis are reported in Table II, and show the varying importance of these shortly living components for different dopants. Namely, these components are well detected in La and Y-doped PWO, while in the Lu-doped one they are practically absent. The overall decrease of the

induced absorption coefficient in the trivalent ion doped PWO is consistent with previous observations at longer times [39] made on the same crystals.

2. 1. 4 Influence of stoichiometry

A systematic study of crystal quality and radiation damage was performed on the set of PWO crystals grown from the melt of different initial stoichiometry (from 49.5 to 50.5 % of PbO in the melt) [40]. The congruent composition of the melt was established at 49.92% of PbO. The minimum of radiation damage was found around 49.7-49.8% of PbO in the melt - Fig. 17, in good agreement with the above value of the congruent composition. The analyses of the crystal composition by microprobe have shown that no solid solutions are created (i.e. no intermediate phases are found between $PbWO_4$, Pb_2WO_5 and WO_3 in the lead rich and lead poor end parts of the crystals, respectively). The absence of solid solutions in PbO-WO_3 system at around 1:1 composition was confirmed also by other authors recently [41].

2.2 Crystals grown by Bridgman method

The Chinese pre-production will start next year and to achieve such a goal, Chinese groups engaged intensive R&D in two different areas: crystal quality optimisation and quantity production considering the reproducibility of the performances [17]. Several crystals produced by SIC and BGRI were tested: we will show and discuss here only a few interesting results on the recent crystal production from both Chinese plants.

The effects of different dopants and treatments on the radiation damage were investigated measuring longitudinal and transversal transmission as well as light yield, before and after irradiation. Irradiation tests and transmission measurements were performed at ENEA- Casaccia Centre (Rome-Italy) while the set-up for light yield loss (that allows to perform measurements immediately after switch-off the irradiation) is installed in PSI-Eichlabor (Switzerland) [42].

The test procedure described above was applied to several batches of undoped and doped PWO crystals [13]. These crystals, typically cut in pairs from the same “father” ingot, underwent a post-growth treatment close to their melting point. Such a treatment is believed to allow compensation of oxygen deficiency. In a first round of optimisations, air and oxygen were used. Annealing in oxygen atmosphere gives a crystal radiation resistant; in a second step, the best annealing cycle in oxygen was selected (48 hours at 850 °C) and in a third round, the reproducibility was proven for samples 5 cm long. The reproducibility of relative LY loss for three different 50 mm long oxygen-annealed crystals was detected. All crystals present losses not more than 2% in LY. After the optimisation of 5 cm long crystals, it is possible to produce full-size crystals with the same procedure.

Fig. 18 shows the longitudinal and transversal transmission for full-size BGRI crystal doped by 50 ppm La^{3+} and oxygen-annealed (BGRI-457). The transversal measurements at different points along the crystals give important information about the longitudinal parameter. For this sample no differences are observed at different distances from the seed and radiation induced absorption coefficient (μ) satisfies the CMS demands (Fig. 18-inset).

As mentioned above, a Chinese producer (SIC) tried to use antimony and a co-doping of lanthanum and antimony ions as doping. Fig. 19 shows longitudinal transmission curves for samples (10 cm long) doped by antimony (SIC-J16) and co-doped by lanthanum and antimony (SIC-234): also in this case the behaviour of μ answers to the CMS specifications as regards the radiation resistance (Fig. 19-inset).

Observing the μ shape shown in Fig. 19, where it is reported a behaviour of PWO:Sb (SIC-J16) and PWO:Sb&La (SIC-234), it is possible to suggest that in the first case (PWO:Sb), antimony plays a role like niobium, i. e. as pentavalent ion (suppression of 620 nm band), while in the second one (PWO:La&Sb) the μ shape is probably due to the superimposition of two typical μ shapes (a decrease of the induce damage over a full spectral range and an appearance of a new band near 520 nm, due typically to the lanthanum (or trivalent) doping) [15].

A few full-size PWO:Sb crystals (produced recently by SIC, SIC-230) were measured and the results obtained for 10 cm long crystals were confirmed (Fig. 20).

3. CONCLUSIONS

The investigation performed during 1998 has allowed to obtain significant results both from the point of view of the optimisation of the scintillation characteristics and on the basic comprehension of the optical properties of the material. With respect to the past, additional experimental techniques as on-line absorption measurements, EPR and low temperature wavelength resolved TSL have been involved too.

By a detailed EPR investigation, the structure of a new paramagnetic electron centre ($(WO_4)^{3-}$) has been described, and its role as electron trap operating at helium temperatures has been clarified by spectrally resolved TSL measurements too. Moreover, the comparison with the optical properties of another tungstate of the same scheelite structure as $CaWO_4$ has provided new insights in the investigation of the role of the Pb cation in the creation of luminescent sites, and on the possible structure of trap levels acting in TSL.

An influence similar to that previously observed in the case of lanthanum doping has been noticed by considering other trivalent ions as Lu, Y and Gd: namely, a strong improvement of the scintillation speed and of the radiation induced absorption has been found in all these cases. Besides the usual techniques, the influence of these dopants has been monitored also by on-line absorption measurements in order to investigate the recovery features also at very short times following irradiation. As the segregation coefficients of these ions are quite different, several doping conditions are available, to be tested on the large scale production of long PWO crystals. Finally, the influence of stoichiometry conditions has been investigated as well, allowing to establish the most suitable percentage composition of PbO in the melt in order to minimize the effects of radiation damage and to increase the crystal quality.

Very interesting results were found using a co-doping with trivalent and pentavalent ions also for full-size crystals produced by BTCP–Russia (Czochralski method) as well as SIC-China (Bridgman method) plants. All full-size crystals produced recently in all production centres satisfy the CMS demands as regards the radiation induced absorption coefficient as well as the light yield loss [18, 19, 42].

At the end of LUMEN activity (1996-1998), we can conclude that significant improvements were obtained on the host matrix material, growth and post-growth procedures as well as the radiation resistance of PWO using trivalent and pentavalent ions doping for Chinese and Russian crystals.

4. REFERENCES

1. S. Baccaro, P. Bohacek, B. Borgia, A. Cecilia, S. Croci, I. Dafinei, M. Diemoz, P. Fabeni, A. Festinesi, O. Jarolimek, E. Longo, M. Martini, E. Mihokova, M. Montecchi, M. Nikl, K. Nitsch, G. Organtini, G.P. Pazzi, G. Spinolo, A. Vedda: *Understanding of $PbWO_4$ scintillator characteristics and their optimisation*, Nota Interna no. 1095, Dept. of Physics, University La Sapienza, Roma, May 18, 1998, see also CMS note 1998/067, CERN, Geneva.
2. M. Nikl, P. Bohacek, K. Nitsch, E. Mihokova, K. Polak, M. Martini, A. Vedda, S. Croci, G.P. Pazzi, P. Fabeni, S. Baccaro, B. Borgia, I. Dafinei, M. Diemoz, G. Organtini, E. Auffray, P. Lecoq, M. Kobayashi, M. Ishii, Y. Usuki, V. Murk, O. Jarolimek, Proc. of SCINT'97, 22 - 25 Sept, 1997, Shanghai, China, p.171.
3. M. Nikl, P. Straková, K. Nitsch, V. Petøíèek, V. Múèka, O. Jarolímek, J. Novák, P. Fabeni, Chem. Phys. Lett. 291, 300 (1998).
4. M. Nikl, P. Bohacek, K. Nitsch, E. Mihokova, M. Martini, A. Vedda, S. Croci, G.P. Pazzi, P. Fabeni, S. Baccaro, B. Borgia, I. Dafinei, M. Diemoz, G. Organtini, E. Auffray, P. Lecoq, M. Kobayashi, M. Ishii, Y. Usuki, Appl. Phys. Lett. 71, 3755 (1997)
5. M. Nikl, K. Nitsch, S. Baccaro, A. Cecilia, M. Montecchi, B. Borgia, I. Dafinei, M. Diemoz, M. Martini, E. Rosetta, G. Spinolo, A. Vedda, M. Kobayashi, M. Ishii, Y. Usuki, O. Jarolimek, R. Uecker, J. Appl. Phys. 82, 5758 (1997)
6. S. Baccaro, P. Bohácek, B. Borgia, A. Cecilia, I. Dafinei, M. Diemoz, M. Ishii, O. Jarolimek, M. Kobayashi, M. Martini, M. Montecchi, M. Nikl, K. Nitsch, Y. Usuki, A. Vedda, phys. stat. sol.(a) 160, R5 (1997).
7. M. Kobayashi, Y. Usuki, M. Ishii, T. Yazawa, K. Hara, M. Tanaka, M. Nikl, K. Nitsch, NIM A399, 261 (1997).

8. M. Kobayashi, Y. Usuki, M. Ishii, T. Yazawa, K. Hara, M. Tanaka, M. Nikl, S. Baccaro, A. Cecilia, M. Diemoz, I. Dafinei, NIM A404, 149 (1998).
9. S. Baccaro, A. Cecilia, S. Croci, I. Dafinei, M. Diemoz, A.E. Borisevich, P. Lecoq, O.V. Kondratiev, M.V. Korzhik, A. Vedda, *Electron centers in lead tungstate crystals*, (in Russian) to be published in Journal of Applied Spectroscopy.
10. ECAL-CMS Technical Design Report "Electromagnetic calorimeter", 4 December 1997.
11. S. Baccaro, B. Borgia, A. Cecilia, I. Dafinei, M. Diemoz, P. Fabeni, M. Nikl, M. Martini, M. Montecchi, G. Pazzi, G. Spinolo, A. Vedda, Nuclear Physics B 61B, 66-70 (1998)
12. P. Lecoq, "Inorganic Scintillator and Their Applications" Ed. By Yin Zhiwen, Li Peijun, Feng Xiqi, Xue Zhilin; Shangai, P. R. China, September, p. 13, 1997.
13. H.F. Chen, K. Deiters, H. Hofer, P. Lecomte, F. Nessi-Tedaldi, NIM A 414, 149-155 (1998).
14. E. Auffray, P. Lecoq, M. Korzhik, A. Annenkov, O. Jarolímek, M. Nikl, S. Baccaro, A. Cecilia, M. Diemoz, I. Dafinei, NIM A 402, 75 (1998)
15. A.N. Annenkov, E. Auffray, M. Korzhik, P. Lecoq, J-P. Peigneux, CMS-NOTE CERN, 1998/041, (1998).
16. S. Baccaro, P. Bohácek, B. Borgia, A. Cecilia, I. Dafinei, M. Diemoz, M. Ishii, O. Jarolimek, M. Kobayashi, M. Martini, M. Montecchi, M. Nikl, K. Nitsch, Y. Usuki, A. Vedda, phys. stat. sol. (a) 164, R9 (1997).
17. D. Yan, in: Tungstate crystals, eds. S. Baccaro, B. Borgia, I. Dafinei, E. Longo, Univ. degli Studi La Sapienza 1999, p. 7 (Proceedings of IW on Tungstate Crystals, Oct 1998, Roma, Italy).
18. P. Lecoq, in: Tungstate crystals, eds. S. Baccaro, B. Borgia, I. Dafinei, E. Longo, Univ. degli Studi La Sapienza 1999, p. 23 (Proceedings of IW on Tungstate Crystals, Oct 1998, Roma, Italy).
19. A.N. Annenkov, A.A. Fedorov, Ph. Galez, V.A. Kachanov, M.V. Korzhik, V.D. Ligun, J.M. Moreau, V.N. Nefedov, V. B. Pavlenko, J.P. Peigneux, T.N. Timoshchenko, B.A. Zadneprovskii, phys. stat. sol. (a) 156, 493 (1996).
20. M. Kobayashi, M. Ishii, Y. Usuki, NIM A 406, 442 (1998).
21. S. Baccaro, P. Bohácek, A. Cecilia, I. Dafinei, M. Diemoz, M. Ishii, M. Kobayashi, M. Montecchi, M. Nikl, K. Nitsch, M. Martini, Y. Usuki, A. Vedda, in: Tungstate crystals, eds. S. Baccaro, B. Borgia, I. Dafinei, E. Longo, Univ. degli Studi La Sapienza 1999, p. 176 (Proceedings of IW on Tungstate Crystals, Oct 1998, Roma, Italy).
22. S. Baccaro, P. Bohácek, A. Cecilia, I. Dafinei, M. Diemoz, P. Fabeni, M. Ishii, M. Kobayashi, V.V. Laguta, M. Martini, F. Meinardi, E. Mihokova, M. Montecchi, M. Nikl, G. Organtini, G.P. Pazzi, J. Rosa, Y. Usuki, A. Vedda, M.I. Zaritskii, in: Tungstate crystals, eds. S. Baccaro, B. Borgia, I. Dafinei, E. Longo, Univ. degli Studi La Sapienza 1999, p. 128 (Proceedings of IW on Tungstate Crystals, Oct 1998, Roma, Italy).
23. Hofstaetter, A. Scharmann, D. Schwabe, B. Vitt, Z. Physik B30, 305 (1978).
24. Hofstaetter, R. Oeder, A. Scharmann, D. Schwabe, B. Vitt, phys. stat. sol. (b) 89, 375 (1978).
25. M. Kobayashi, M. Ishii, K. Harada, Y. Usuki, H. Okuno, H. Shimizu, T. Yazawa, NIM A 373, 333 (1996).
26. V.V. Laguta, J. Rosa, M.I. Zaritskii, M. Nikl, Y. Usuki, J. Phys. Cond. Mat. 10, 7293 (1998).
27. M. Bohm, F. Henecker, A. Hofstaetter, M. Luh, B.K. Meyer, A. Scharmann, O.V. Kondratiev, M.V. Korzhik, *Electron traps in the scintillator material PbWO4 and their correlation to thermally stimulated luminescence*, Proc. of Eurodim98, July 1998, Keele, England (Rad. Eff. Def. Sol. 1999).
28. M. Martini, G. Spinolo, A. Vedda, M. Nikl, K. Nitsch, V. Hamplova, P. Fabeni, G.P. Pazzi, I. Dafinei, P. Lecoq, Chem. Phys. Lett. 260, 418 (1996).
29. M. Herbert, A. Hofstaetter, T. Nickel, A. Scharmann, phys. stat. sol. (b) 141, 523 (1987).
30. L.A. Kappers, F. Dravnieks, J.E. Wertz, J. Phys. C 7, 1387 (1974).
31. M. Martini, F. Meinardi, G. Spinolo, A. Vedda, M. Nikl, Y. Usuki, *Investigation of shallow traps in $PbWO_4$ by wavelength resolved Thermally Stimulated Luminescence*, accepted in Physical Review B.

32. S. Croci, M. Martini, G. Spinolo, A. Vedda, M. Nikl, P. Bohacek, S. Baccaro, M. Diemoz, Y. Usuki, R. Uecker, *Trap levels and emission centres in PbWO4 and CaWO4 single crystals*, Proc. of Eurodim98, July 1998, Keele, England (Rad. Eff. Def. Sol. 1999).

33. M. Martini, E. Rosetta, G. Spinolo, A. Vedda, M. Nikl, K. Nitsch, I. Dafinei, P. Lecoq, J. Lumin. 72-74, 689 (1997).

34. Y. Zhang, W.A.N. Holzwarth, R.T. Williams, Phys. Rev. B 57, 12738 (1998).

35. R.Y. Zhu, Q. Deng, H. Newman, C.L. Woody, J.A. Kierstead, S.P. Stoll, IEEE Trans. Nucl. Sci. 45, 686 (1998).

36. E. Auffray, I. Dafinei, F. Gautheron, O. Lafond-Puyet, P. Lecoq, M. Schneegans, in: Inorganic Scintillators and their applications, eds. P.Dorenbos, C.W. van Eijk, Delft University Press 1996, p. 282 (Proc. of SCINT`95, Aug 28 - Sep 1, 1995, Delft, The Netherland).

37. L. Nagornaya, A. Apasenko, V. Ryzhikov, I. Tupitsina, N. Golubev, IEEE Trans. Nucl. Sci. 44, 866 (1997).

38. M. Sulc, M. Vognar, E. Simane, O. Jarolimek, M. Finger, M. Nikl, S. Baccaro, M. Diemoz, in: Tungstate crystals, eds. S. Baccaro, B. Borgia, I. Dafinei, E. Longo, Univ. degli Studi La Sapienza 1999, p. 216 (Proceedings of IW on Tungstate Crystals, Oct 1998, Roma, Italy).

39. S. Baccaro, B. Borgia, A. Cecilia, I. Dafinei, M. Diemoz, M. Nikl, M. Montecchi, Radiat. Phys. Chem. 52, 635-638, 1998.

40. P. Bohacek, M. Nikl, J. Novak, Z. Malkova, B. Trunda, J. Rysavy, S. Baccaro, A. Cecilia, I. Dafinei, M. Diemoz, K. Jurek, in: Tungstate crystals, eds. S. Baccaro, B. Borgia, I. Dafinei, E. Longo, Univ. degli Studi La Sapienza 1999, p.56 (Proceedings of IW on Tungstate Crystals, Oct 1998, Roma, Italy).

41. K. Tanij, M. Ishii, Y. Usuki, M. Kobayashi, K. Hara, H. Takano, N. Senguttuvan, in: Tungstate crystals, eds. S. Baccaro, B. Borgia, I. Dafinei, E. Longo, Univ. degli Studi La Sapienza 1999, p. 62 (Proceedings of IW on Tungstate Crystals, Oct 1998, Roma, Italy).

42. S**.** Baccaro*, Recent progress in the development of lead tungstate crystals*, to be published in IEEE- Trans. Nucl. Sc.

5. FIGURE CAPTIONS

Fig.1 - The intitial transmission for the set of doped japanese PWO samples at RT.

Fig.2 - Radiation induced absorption spectra (^{60}Co irradiation about 300 Gy) for the set of doped japanese PWO samples at RT.

Fig.3 - The dependence of induced abosrption coefficient at 420 nm on the irradiation dose for the set of doped japanese PWO samples at RT.

Fig.4 - Photoluminescence decays at 500 nm under excimer laser excitation (308 nm XeCl line) at RT for selected doped japanese PWO samples.

Fig.5 - Thermoluminescence glow curves after irradiation at 90 K by X-rays for selected doped japanese PWO samples.

Fig.6 - Thermoluminescence glow curves after irradiation at 295 K by X-rays for selected doped japanese PWO samples.

Fig.7 - Induced absorption spectra (after 241 Gy dose) of PWO:Gd Prague for 20,40 and 80 molar ppm concentration of Gd in the melt at RT.

Fig.8 - TSL glow curves of PWO:Gd Prague for 20,40 and 80 molar ppm concentration of Gd in the melt after X-ray irradiation at RT.

Fig.9 - Excimer laser (XeCl 308 nm line) excited photoluminescence decay at 400 nm and RT of three PWO:Gd samples with 20, 40 and 80 ppm in the melt grown in Prague.

Fig.10 - EPR characteristics of undoped japanese sample after UV irradiation (for the details see Ref. 15).

Fig.11 - TSL glow curves after X-irradiation at 9 K at undoped and La-doped japanese samples (the former sample is identical with that related to Fig. 9).

Fig.12 - TSL glow curves of A) undoped; B), La-doped $PbWO_4$ after x-ray irradiation. The inset shows the emission spectrum of the TSL of the undoped sample integrated in the 20-100 °C temperature region.

Fig.13 - TSL glow curves of A) undoped; B), La-doped $CaWO_4$ after x-ray irradiation. The inset shows the emission spectrum of the TSL of the undoped sample integrated in the 20-100 °C temperature region.

Fig.14 - Wavelength resolved TSL of undoped $CaWO_4$ following X-ray irradiation at 90 K.

Fig.15 - Induced absorption spectra resolved in time and wavelength of 15 cm long undoped (L24) and La-doped (L23) PWO crystals produced by CRYTUR, Preciosa a.s. resulting from on-line measurements under microtrone irradiation at RT (for the details see Ref. 28).

Fig.16 - Cuts in time related to on-line measurements of induced absorption at 420 nm under microtorone irradiation (see 2.3 and Fig. 14) for undoped and La, Y and Lu doped 15 cm long PWO samples produced by CRYTUR, Preciosa a.s.

Fig.17 - Dependence of induced absorption coefficient at 420 nm for different initial stoichiometry of the melt used for the growth of PWO (irradiation dose about 100 Gy).

Fig.18 - Longitudinal (lower continuous line) and transversal transmissions at various distances from seed for PWO:La oxygen-annealed crystal (BGRI-457) from BGRI. Radiation induced absorption coefficient after 56.4 Gy absorbed dose (at 3.76 Gy/h) (inset)

Fig.19 - Longitudinal transmission for PWO:Sb (SIC-J16) and PWO:Sb&La (SIC-234) crystals (L=10 mm). Radiation induced absorption coefficient after 250 Gy absorbed dose (at 3.91 Gy/h).

Fig.20 - a) Longitudinal transmission curves for PWO:Sb crystal (SIC230-L=231.6 mm) after different irradiation doses (3.91 Gy/h). b) Rad. ind. abs .coeff. for PWO:Sb crystal (SIC230) after 69.35 Gy irradiation dose (3.91 Gy/h).

Table I

Influence of different dopants on TSL and scintillation characteristics of PWO crystals.

Sample	τ_{mean} [ns] PL	τ_{mean} [ns] SC	I^{160}/I^{350} TSL[a.u.]	LY [phel/MeV]	c_X [at.ppm]
P-Pb	22	7.7	.032/.042	37	undoped
P-Sc	20	6.2	.136/.153	37	51
P-Gd	8	6.0	6.27/6.27	33	175[#]
P-Lu	12	5.7	2.42/2.55	37	45[#]
P- Y	12	5.4	4.41/4.42	40	110[#]
P-Nb	112	11.1	1.08/1.12	26	670

[#] The values are calculated using segregation coefficient value (see the text).

Table II

The 2-exponential fit of $\mu(t)= \Sigma\, a_i \exp[-t/\tau_i]$, i=2, τ_i in [s] of induced absorption coefficient time course related to the on-line transmission measurements (see 2.3 and Fig. 15).

Sample	$\mathbf{a_1}$	$\boldsymbol{\tau_1}$**[s]**	$\mathbf{a_2}$	$\boldsymbol{\tau_2}$**[s]**
Lu-doped	-	-	1	61600
undoped	0.32	320	2.83	53000
La-doped	0.32	290	1.14	9290
Y-doped	0.32	140	1.57	4300

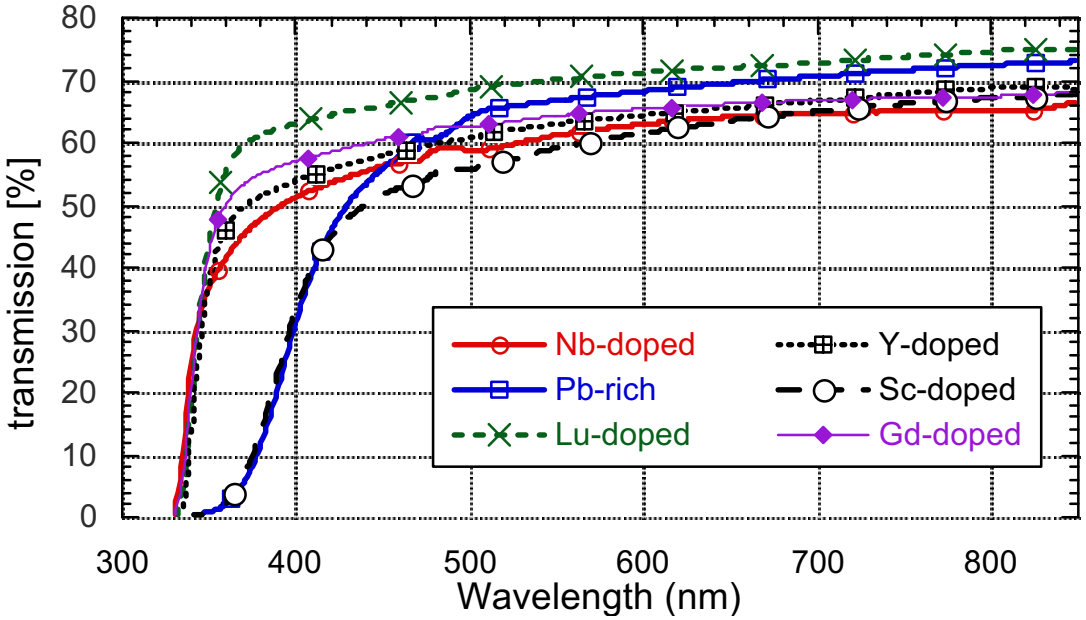
transmission [%]
Wavelength (nm)
Nb-doped
Pb-rich
Lu-doped
Y-doped
Sc-doped
Gd-doped

Fig. 1

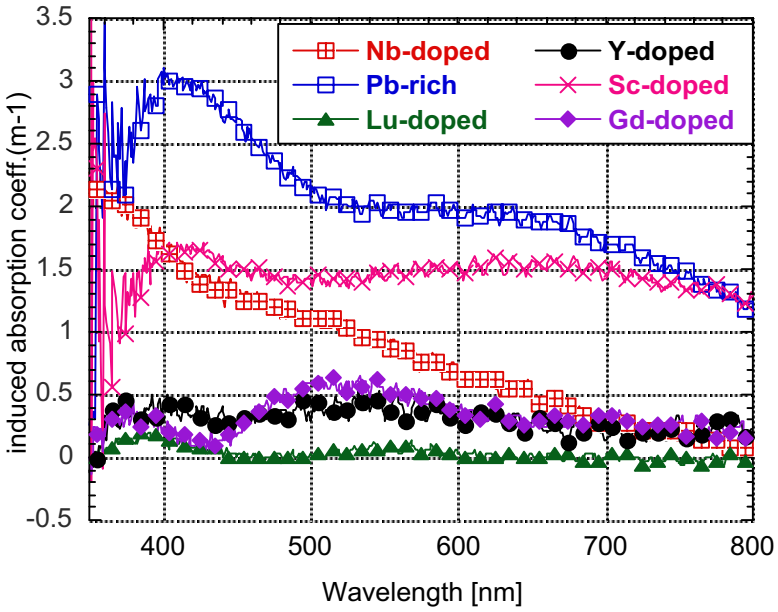
induced absorption coeff.(m-1)
Wavelength [nm]
Nb-doped
Pb-rich
Lu-doped
Y-doped
Sc-doped
Gd-doped

Fig. 2

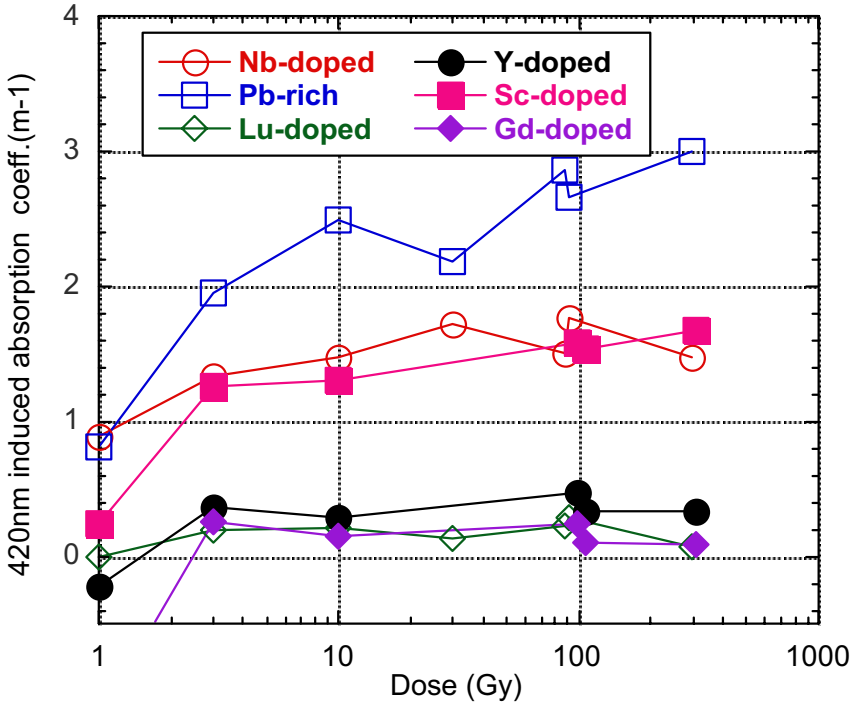
Nb-doped
Pb-rich
Lu-doped
Y-doped
Sc-doped
Gd-doped
420nm induced absorption coeff.(m-1)
Dose (Gy)
0
1
2
3
4
1
10
100
1000

Fig.3

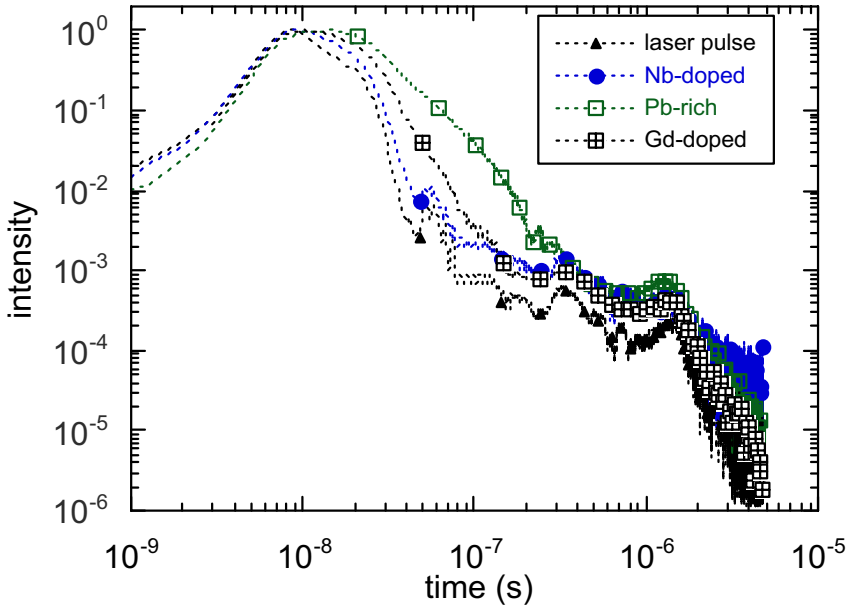
laser pulse
Nb-doped
Pb-rich
Gd-doped
intensity
time (s)
10^{0}
10^{-1}
10^{-2}
10^{-3}
10^{-4}
10^{-5}
10^{-6}
10^{-9}
10^{-8}
10^{-7}
10^{-6}
10^{-5}

Fig. 4

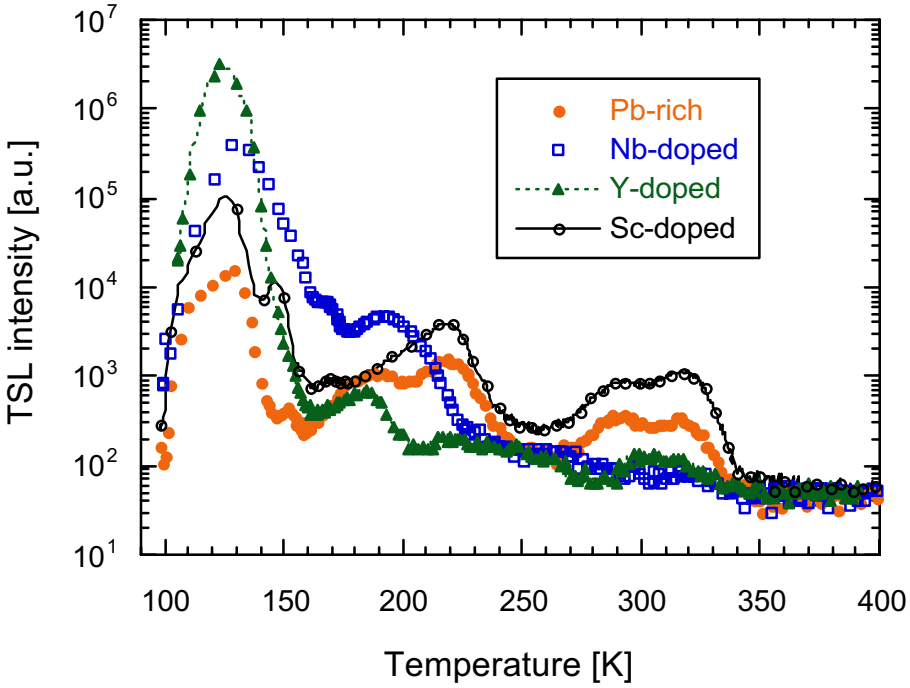
TSL intensity [a.u.]
Temperature [K]
Pb-rich
Nb-doped
Y-doped
Sc-doped

Fig. 5

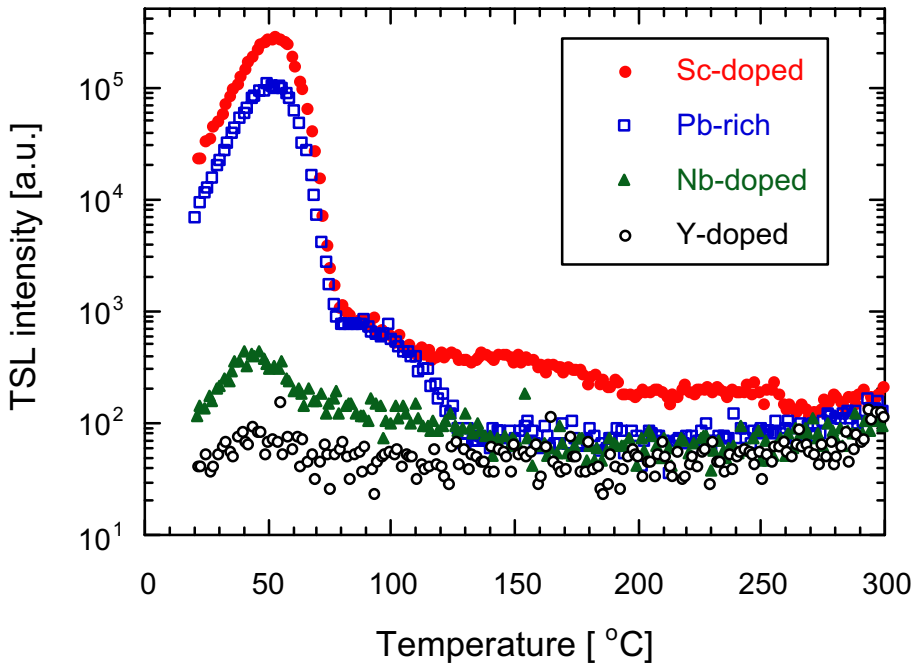
TSL intensity [a.u.]
Temperature [°C]
Sc-doped
Pb-rich
Nb-doped
Y-doped

Fig.6

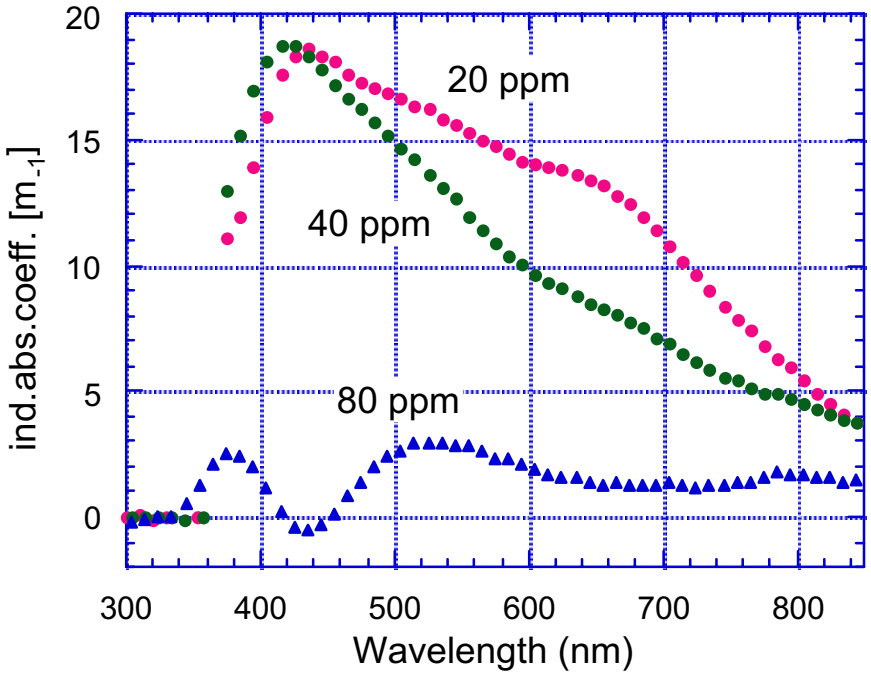
20
15
10
5
0
ind.abs.coeff. [m-1]
20 ppm
40 ppm
80 ppm
300
400
500
600
700
800
Wavelength (nm)

Fig. 7

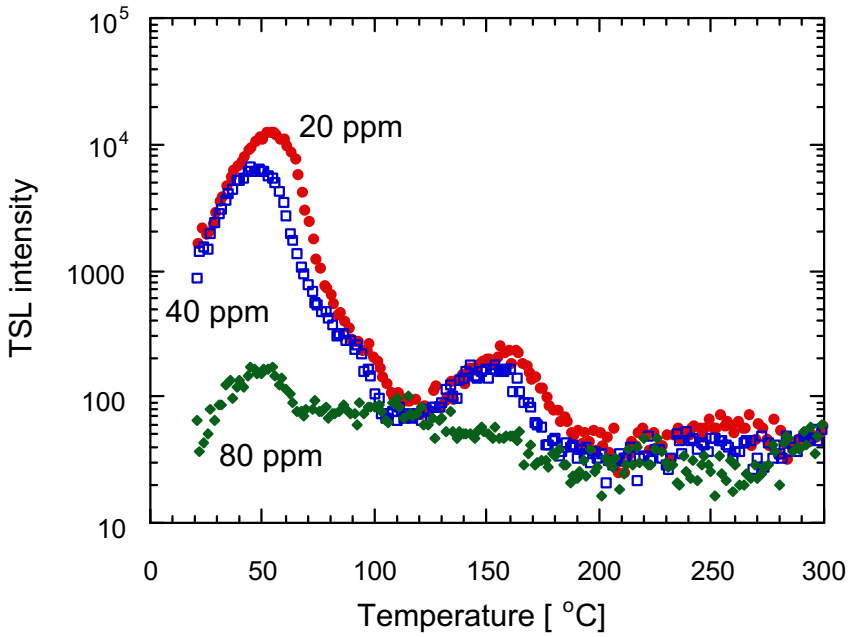
10^5
10^4
1000
100
10
TSL intensity
20 ppm
40 ppm
80 ppm
0
50
100
150
200
250
300
Temperature [°C]

Fig. 8

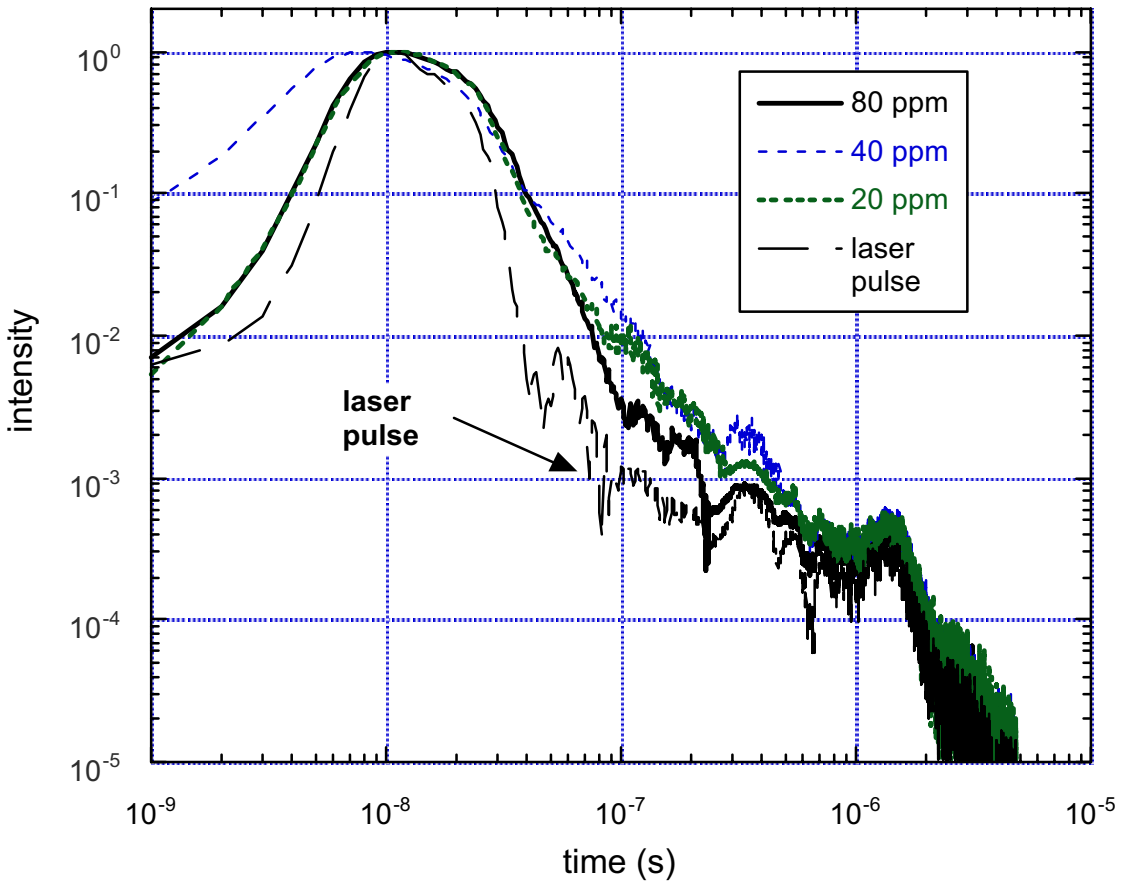
intensity
time (s)
80 ppm
40 ppm
20 ppm
- laser pulse
laser pulse
10^0
10^-1
10^-2
10^-3
10^-4
10^-5
10^-9
10^-8
10^-7
10^-6
10^-5

Fig. 9

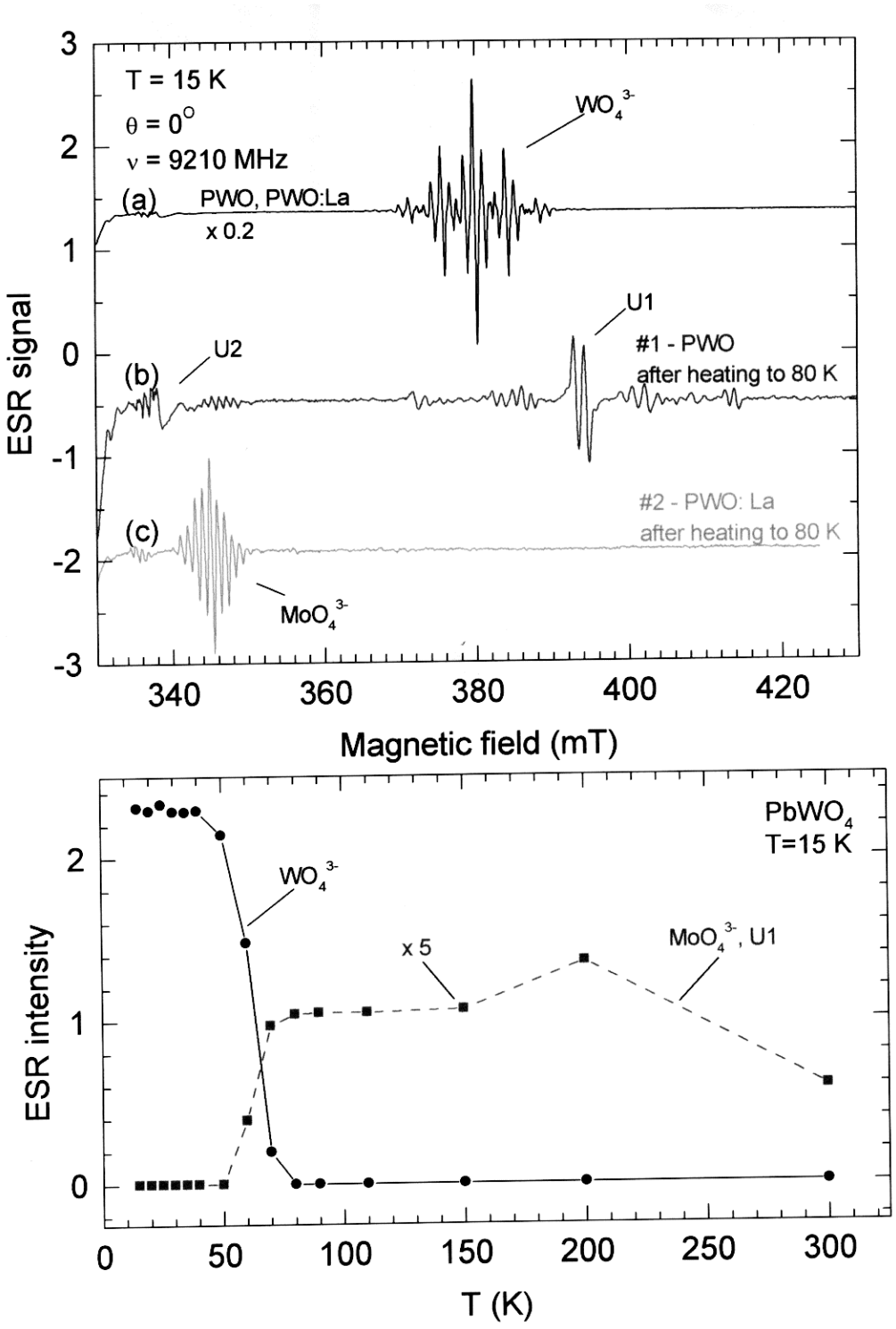
T = 15 K
θ = 0°
ν = 9210 MHz
(a) PWO, PWO:La
x 0.2
WO4 3-
U1
#1 - PWO
after heating to 80 K
U2
(b)
(c)
#2 - PWO: La
after heating to 80 K
MoO4 3-
ESR signal
Magnetic field (mT)
PbWO4
T=15 K
WO4 3-
x 5
MoO4 3-, U1
ESR intensity
T (K)

Fig. 10

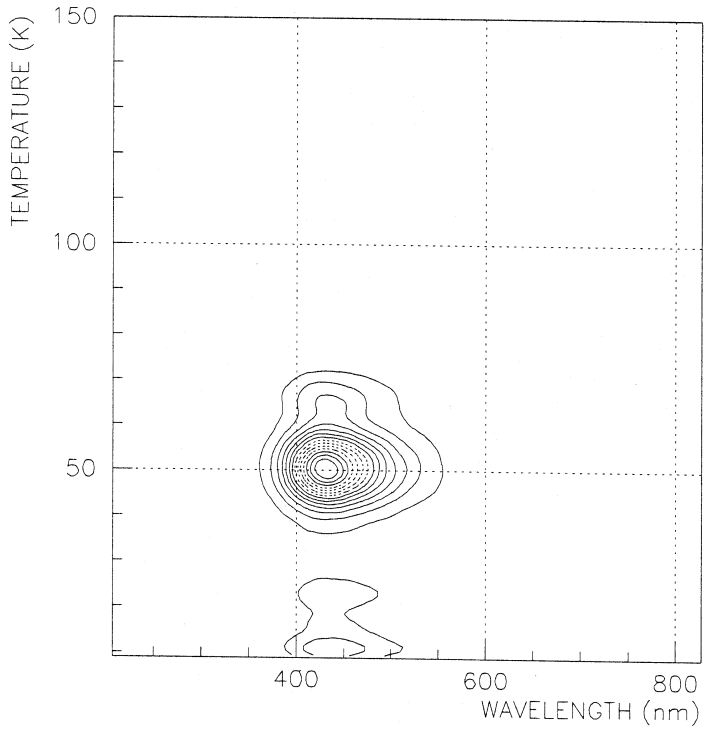
150
100
50
TEMPERATURE (K)
400
600
800
WAVELENGTH (nm)

A)

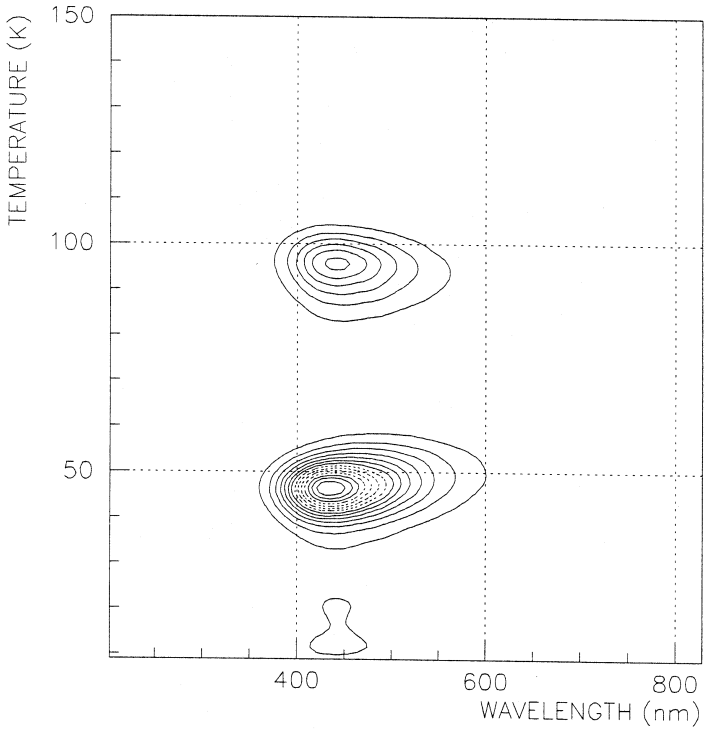
150
100
50
TEMPERATURE (K)
400
600
800
WAVELENGTH (nm)

B)

Fig. 11

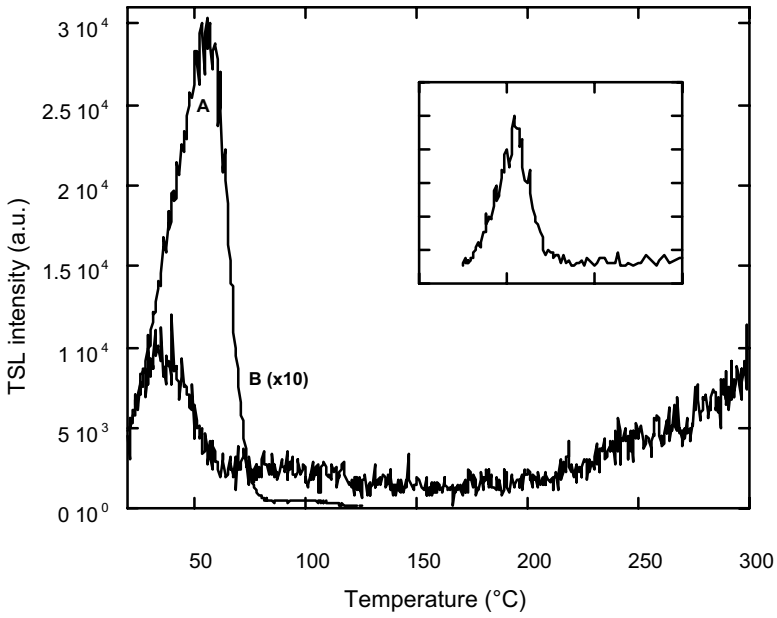
3 10^4
2.5 10^4
2 10^4
1.5 10^4
1 10^4
5 10^3
0 10^0
TSL intensity (a.u.)
A
B (x10)
50
100
150
200
250
300
Temperature (°C)

Fig. 12

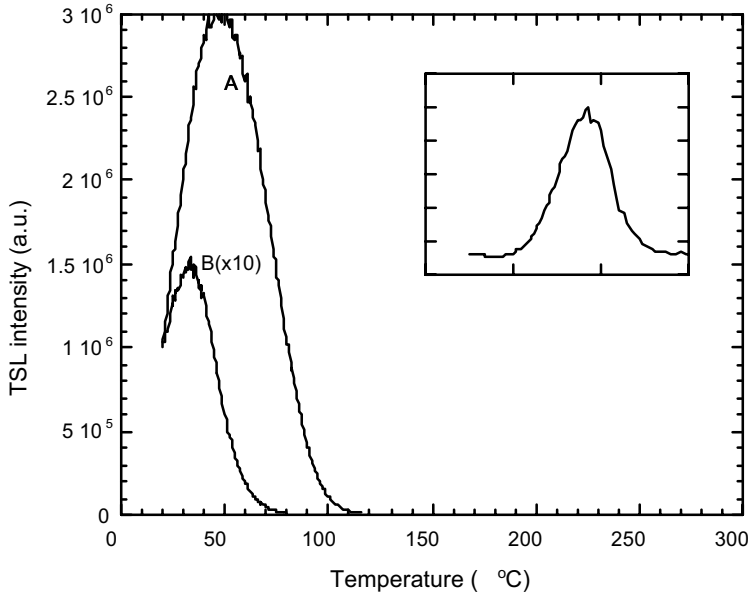
3 10^6
2.5 10^6
2 10^6
1.5 10^6
1 10^6
5 10^5
0
TSL intensity (a.u.)
A
B(x10)
0
50
100
150
200
250
300
Temperature (°C)

Fig. 13

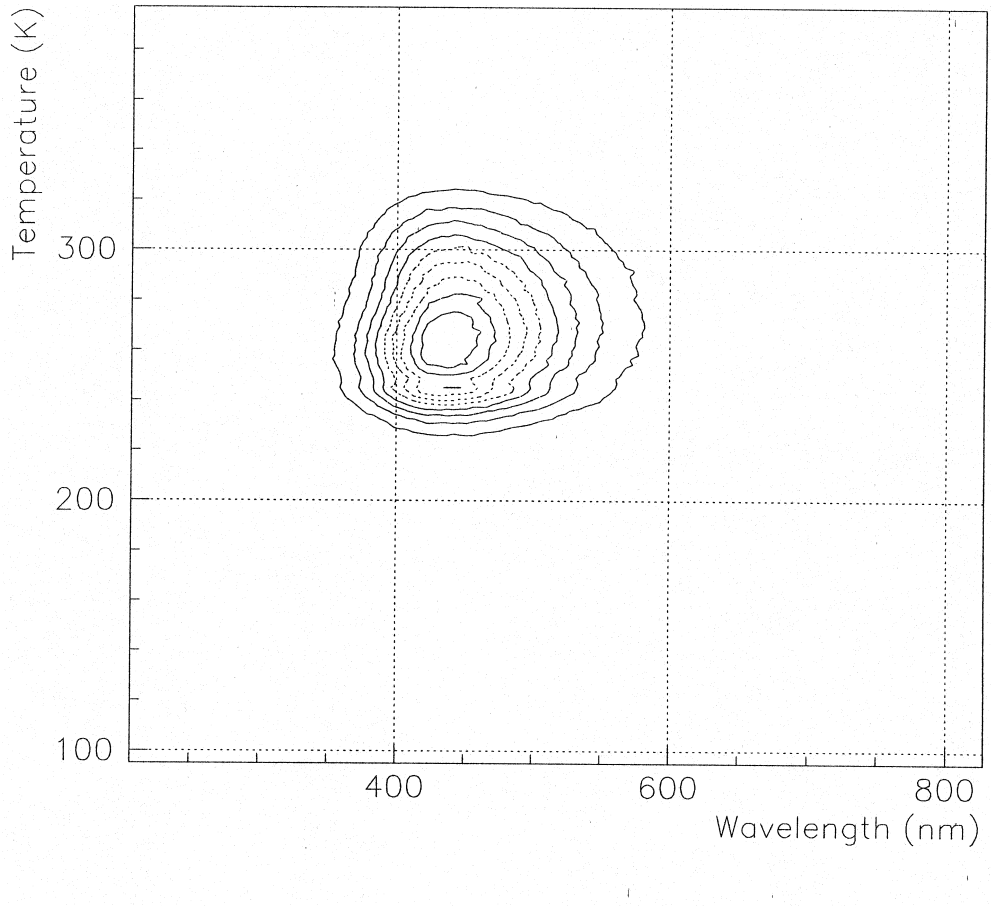

Fig. 14

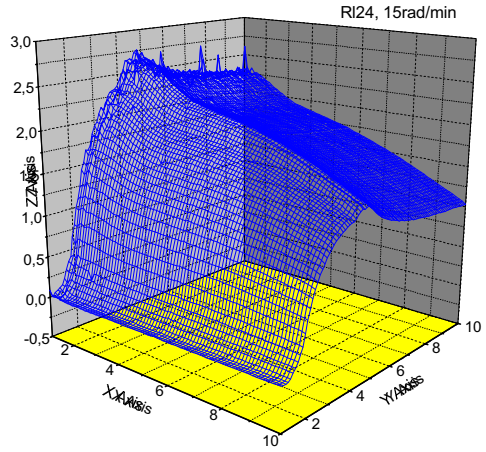
Rl24, 15rad/min
3,0
2,5
2,0
1,5
1,0
0,5
0,0
-0,5
ZZ Axis
2
4
6
8
10
XXAxis
2
4
6
8
10
YYAxis

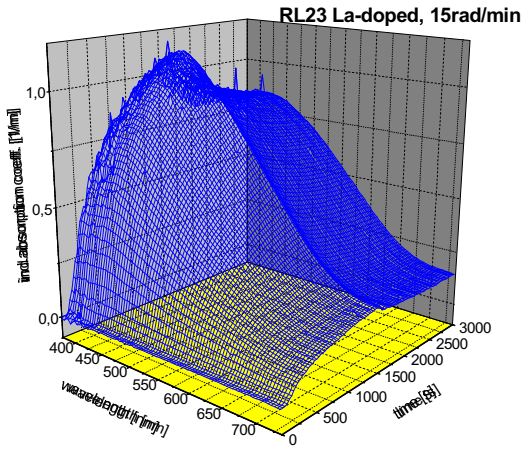
RL23 La-doped, 15rad/min
1,0
0,5
0,0
400
450
500
550
600
650
700
3000
2500
2000
1500
1000
500
0

Fig. 15

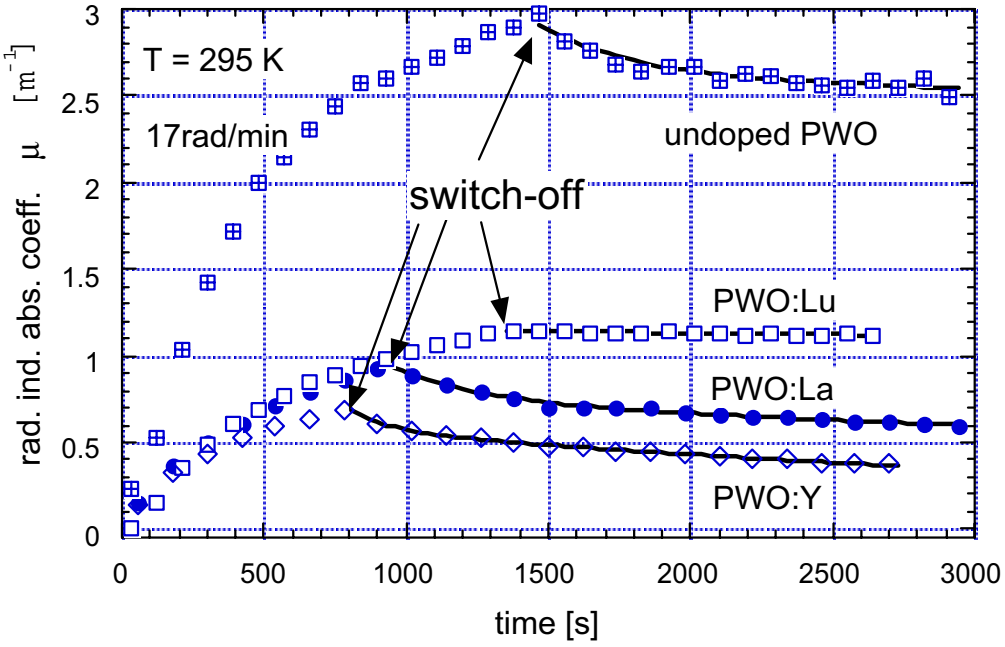
T = 295 K
17rad/min
undoped PWO
switch-off
PWO:Lu
PWO:La
PWO:Y
rad. ind. abs. coeff. μ [m⁻¹]
time [s]
0
0.5
1
1.5
2
2.5
3
0
500
1000
1500
2000
2500
3000

Fig. 16

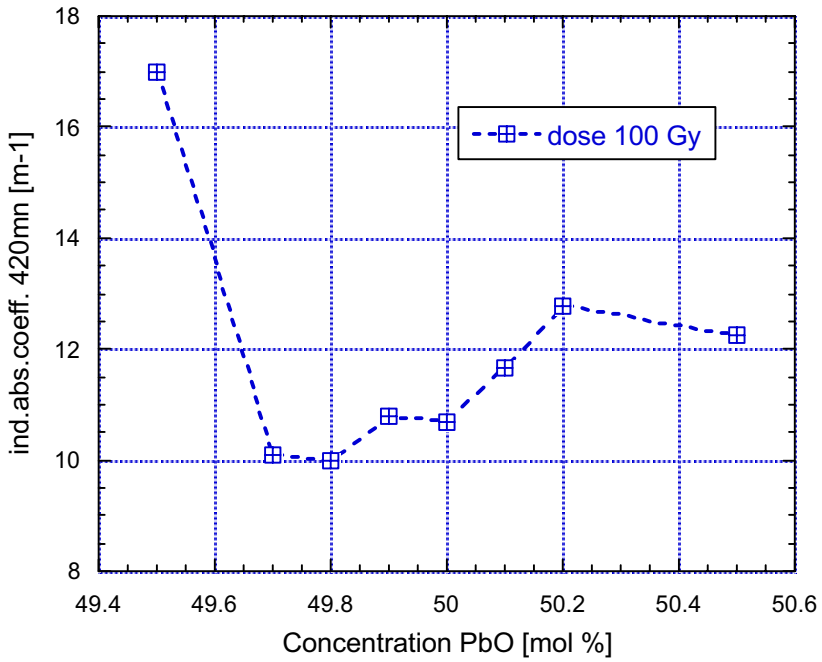
dose 100 Gy
ind.abs.coeff. 420mn [m-1]
Concentration PbO [mol %]
8
10
12
14
16
18
49.4
49.6
49.8
50
50.2
50.4
50.6

Fig. 17

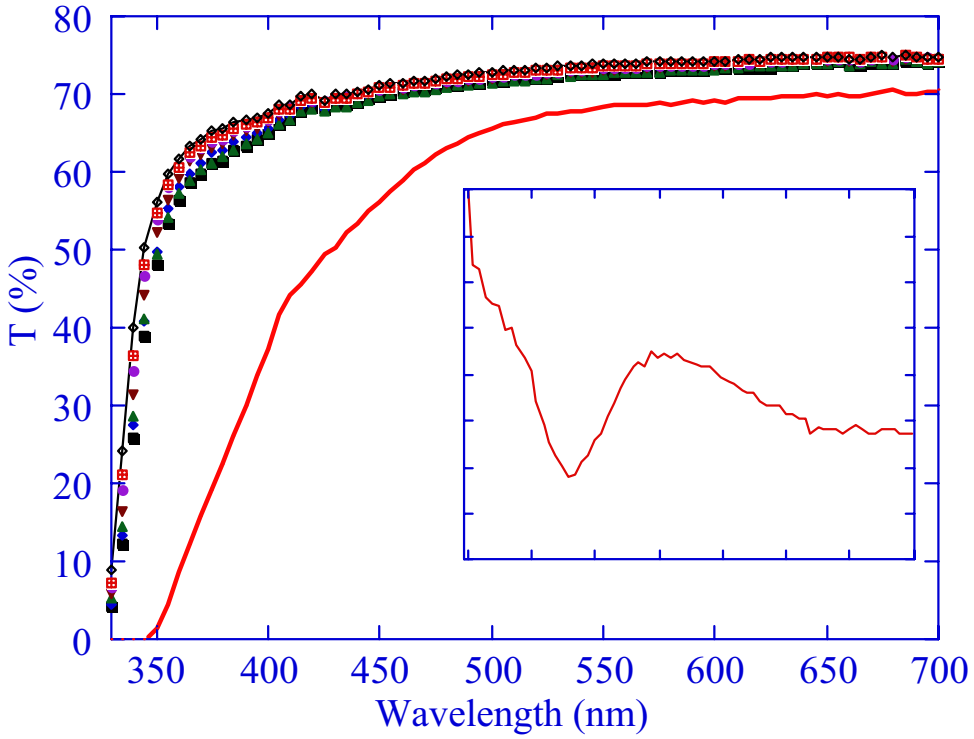
80
70
60
50
40
30
20
10
0
T (%)
350
400
450
500
550
600
650
700
Wavelength (nm)

Fig.18

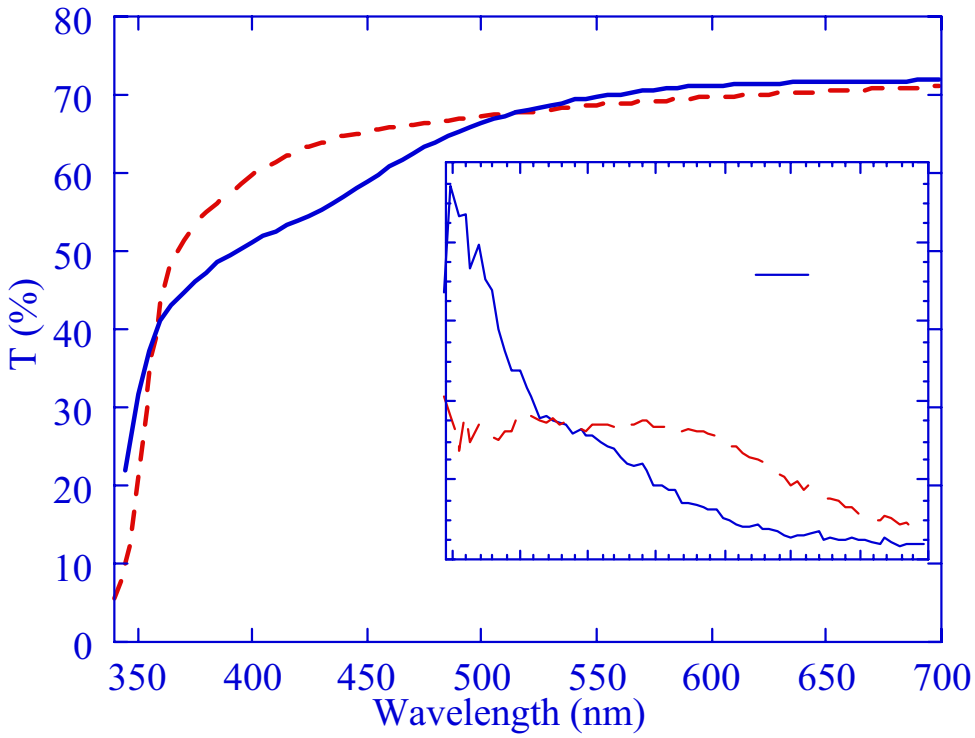
80
70
60
50
40
30
20
10
0
T (%)
350
400
450
500
550
600
650
700
Wavelength (nm)

Fig. 19

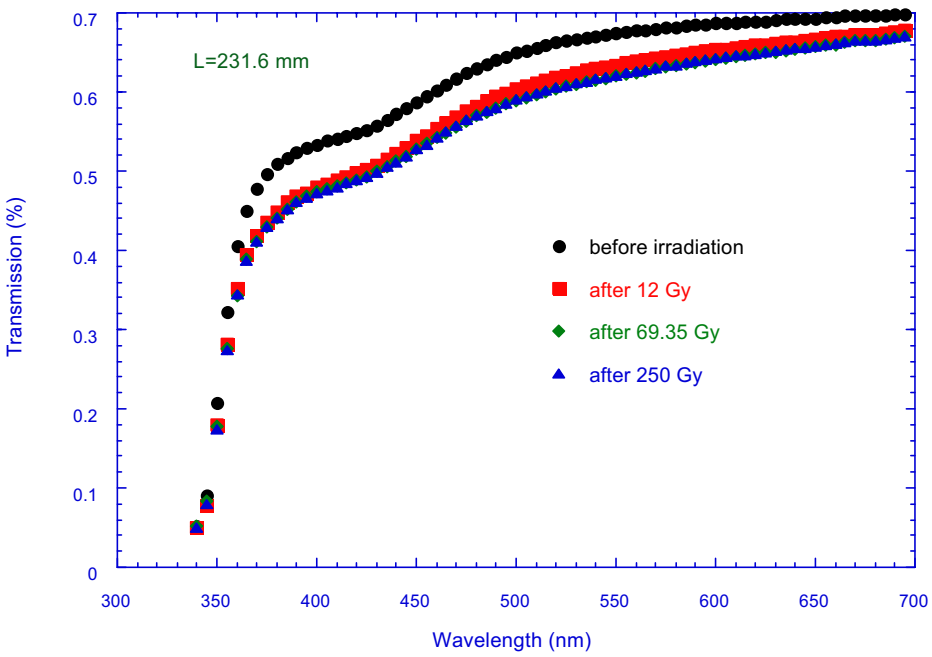

Fig. 20 a

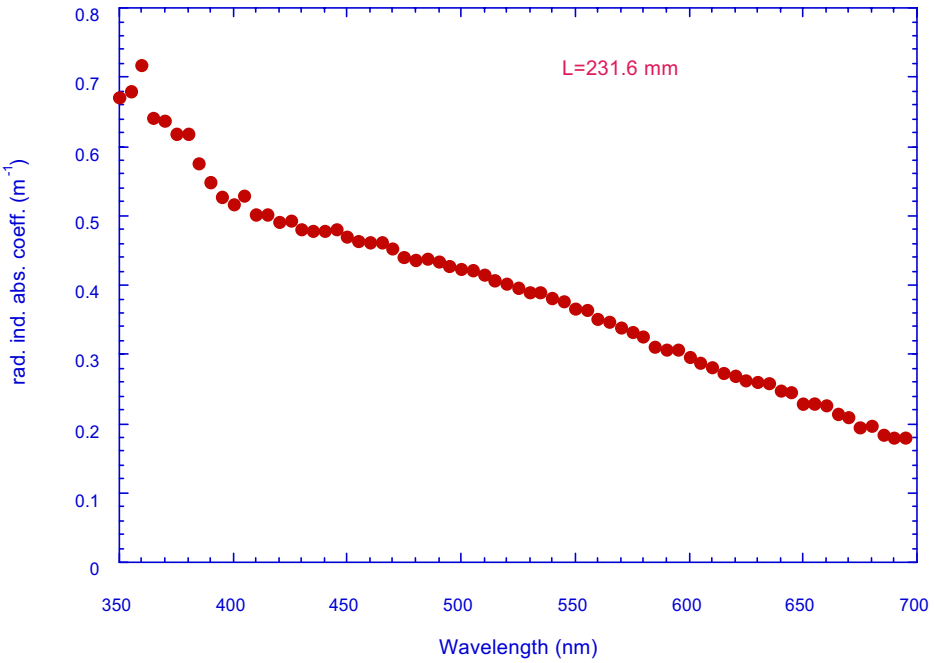

Fig. 20 b